AUSTRALIAN JOURNAL OF BASIC AND APPLIED SCIENCES

ISSN:1991-8178 EISSN: 2309-8414
Journal home page: www.ajbasweb.com

Synthesis of Polyethylenimine-magnetic amorphous carbon nano composite as a novel adsorbent for Hg (II) from aqueous solutions

Mona El-Sayed Eid

Department of Analysis and Evaluation, Egyptian Petroleum Research Institute, Cairo, Egypt.

Address For Correspondence: Mona El-Sayed Eid Department of Analysis and Evaluation, Egyptian Petroleum Research Institute, Cairo , Egypt.
E-mail: dr.monaelsayed2005@yahoo.com

ARTICLE INFO

Article history:
Received 6 October 2016
Accepted 15 November 2016
Published 31 December 2016

Keywords:
Poly(ethyleneimine)- magnetic amorphous carbon - Hg (II) Adsorption - Isotherm- Kinetics - Thermodynamics

ABSTRACT

PEI (polyethylenimine) functionalized magnetic amorphous carbon thin film nano composite (Fe3O4-PEI-ACTF NC), was successfully synthesized and characterized by High Resolution Transmission Electron Microscope (HR-TEM), X-ray diffraction (XRD), Fourier-transform infrared spectrometer (FTIR), and Thermo gravimetric analysis (TGA). The synthesized nano composite Fe3O4-PEI-ACTF was developed as a highly efficient adsorbent for Hg(II) from aqueous samples. Effect of pH, contact time, adsorbent dose, initial concentration and temperature were investigated and optimized through batch adsorption technique. Besides, good magnetic performance of Fe3O4-PEI-ACTF NC makes it easily recovered from water with magnetic separation at low magnetic field. The adsorption kinetic data described well with the pseudo-second-order model and the equilibrium data fitted well to Langmuir isotherm model. The maximum adsorption capacity was 714 µgg-1 for Hg(II). Thermodynamic studies ($\Delta Go < 0$, $\Delta Ho > 0$, $\Delta So > 0$) implied an endothermic and spontaneous adsorption process in nature. Furthermore, the excellent reproducibility indicated that Fe3O4-PEI-ACTF NC has a promising application for removing heavy metals from aqueous environments due to high adsorption capacity and easily and quick separation.

INTRODUCTION

Heavy metal ions such as Pb^{2+}, Cd^{2+}, Hg^{2+}, Ni^{2+}, and Cu^{2+} are very harmful environmental pollutants because they are highly toxic at low concentrations and can accumulate in living organisms, causing several disorders and diseases (Zhou *et al*. 2009; Wang *et al*. 2010). Mercury (Hg) is a bioaccumulative and exceptionally destructive significant metal that causes genuine human medical impacts even at low concentrations. Extreme harm has been reported to the sensory system, kidneys, and different organs after Hg exposure. Agency for Toxic Substances and Disease Registry (ATSDR) considered Hg is one of the "priority hazardous substances" which is released into the environment by both natural processes and human activities (Harris *et al*. 2003; Xiaofang *et al*. 2014). Different industries including electrical and electronics manufacturing plants, chloro-soluble base plants, and sulfide ore roasting operations cause Hg water contaminated (Wang *et al*. 2010; Parham *et al*. 2012). An economic and simple effective method was required for treatment of the wastewater containing Hg(II).

The main techniques that have been used on metal content reduction from industrial waste are chemical precipitation, ion exchange, membrane filtration, electrolytic methods, reverse osmosis, solvent extraction, and adsorption. However, these methods are limited by high operational cost and/or may be also be inefficient in the removal of some toxic metal ions, mainly at trace level concentrations (Nasirimoghaddam *et al*. 2015). Adsorption is perceived as an efficient and economic technique (Wang *et al*. 2013; Hajipour *et al*. 2010), its efficiency significantly depends on the adsorbent properties and hence, developing an efficient adsorbent is of

To Cite This Article: Mona El-Sayed Eid, Synthesis of Polyethylenimine-magnetic amorphous carbon nano composite as a novel adsorbent for Hg (II) from aqueous solutions ***Aust. J. Basic & Appl. Sci.,*** *10(18), 323-335, 2016*

imperative significance. Numerous novel adsorbents, for example nanomaterials, ion imprinted material, mesoporous materials, carbon nanotubes and magnetic nanoparticles have been utilized. Nanometer-sized materials have gained much attention, because of their distinct chemical, physical and biological properties and because of their high surface area, they can adsorb metal ions with high adsorption capacity (Cheng *et al*. 2012; Jianga *et al*. 2012). In recent years, application of magnetic nanoparticles (MNPs) to adsorb contaminants from aqueous or gaseous effluents has received considerable attention, due to their excellent physical and chemical properties, high surface area, simple separation using external magnetic fields (Panneerselvam *et al*. 2011; Yong-Meia *et al*. 2010). Magnetic iron oxide nanoparticles (Fe_3O_4) have demonstrated broad applications as solid phase adsorbent for removal of different types of pollutants, for example, dyes and heavy metals since no centrifugation or filtration of the sample was needed after treatment (in comparison with non-magnetic adsorbents) (Parham *et al*. 2012). Magnetic iron oxide nanoparticles (Fe3O4) are tend to shape totals because of their magnetic attractive forces and the Vander Waals attractive forces, which cause extreme difficulty in stabilizing the magnetic colloidal dispersion in solutions (Bagheri *et al*. 2012). Several methods have been developed to improve the stability, biocompatibility, and manipulation of the nanoparticles and to minimize their co-aggregation, such as supporting of magnetite nanoparticles on polymers or inorganic matter, like porous silica, amorphous carbon, and zeolites (Larraza *et al*. 2012).

Amorphous activated carbon thin film (ACTF) is a carbonaceous material prepared from agriculture wastes in the form of multiple accumulated sheets, having winding surface. Due to its excellent surface properties, ACTF has been used as support for hybrid nanomaterials (El-Sayed *et al*. 2016).

Polyethylenimine (PEI), which is composed of a large number of primary and secondary amine groups in a molecule, exhibits good adsorption ability for heavy metals (Ghoul *et al*. 2003; Deng and Ting 2005). Furthermore, it is charged over a wide pH range. Therefore, PEI can bind with heavy metal ions through complexation or electrostatic interaction (Pang 2011a; 2011b). The presence of NH_2 groups in PEI molecules will enable the PEI-capped magnetic particles to have good biocompatibility and good solubility in aqueous solutions. The NH_2 groups demonstrated excellent ability to remove heavy metal ions such as Cu(II), Co(II), Ni(II), Zn(II), Pb(II), Cr(VI), and Cd(II) from aqueous solutions (Larraza *et al*. 2012; Ghoul *et al*. 2003; Deng and Ting, 2005; Pang *et al*. 2011b; Xitong *et al*. 2015; Lu *et al*. 2015) due to the strong metal complexing ability of amino groups to the surface of adsorbent.

In the present work, magnetite nanoparticles (Fe_3O_4) were incorporated and dispersed among the ACTF sheets, modified by polyethylenimine (PEI) with functional groups that later affords the growth and stabilization of the magnetic particles. The nono composite Fe_3O_4-PEI-ACTF prepared, was characterized using different techniques such as transmission electron microscopy (TEM), X-Ray diffraction (XRD), Fourier transform infrared (FTIR), and TGA analysis. The ability of the prepared nano composite (Fe_3O_4-PEI-ACTF) to remove Hg(II) from water was investigated, and the adsorption experiments were carried out through batch technique. The synthesized nano composite has full advantage of the characteristics of specific physical, chemical and surface properties of ACTF, selective attachment of amino group and the magnetic separation performance of Fe_3O_4.

2. Experimental:

2.1. Chemicals and materials:

All chemical reagents used were analytical reagent grade, purchased from Sigma–Aldrich Co. Standard Stock solutions of Hg(II) containing 1000 mgL^{-1} were prepared from mercuric nitrate ($Hg(NO_3)_2$ salt and diluted further with deionized water to obtain the lower concentration solutions.

2.2. Preparation of Magnetite–Polyethylenimine–Amorphous Carbon Thin Film Nano Composite (Fe_3O_4–PEI–ACTF NC):

Amorphous carbon thin film (ACTF) was prepared according to El-Sayed *et al*. 2016. Briefly, 50 g of oil palm leaves was washed with deionized water, dried, crushed, and sieved to 0.1- 0.07mm. The crushed OPL was impregnated by 50 ml concentrated sulphuric acid and vigorously stirred for 30 minutes in the presence of 1 g active silica; the resulting residue was subjected for semi-carbonization step using a microwave oven at 450 watts for 20 minutes. Later, the semi-carbonized OPL was subjected to react with cobalt silicate nanoparticle as a catalyst under the addition of concentrated sulfuric acid and heated up to 323 K for 30 minutes. The resultant product as amorphous carbon thin film (ACTF) was washed and vacuum dried at 333 K for 24 h. The final ACTF product was stored until used.

Magnetite nanoparticles (Fe_3O_4 NPs) were prepared by co-precipitation of the $Fe^{3+}$and Fe^{2+}ions by ammonia solution and treating under hydrothermal conditions. Chemical precipitation was achieved at 298 K under vigorous stirring by adding NH4OH solution. The precipitates were heated at 353 K for 30 min, washed several times with water and ethanol, and then finally dried in a vacuum oven at 343 K (Mohapatra *et al*. 2007).

The Fe_3O_4–PEI–ACTF composite material was prepared according to Ying *et al*. 2014, equal amount of ACTF and Fe_3O_4 nano particles suspension solutions in 50 ml methanol were sonicated for 1 h in a water bath

(Elmar 50 Hz) at room temperature. Then, they added to 100 ml 10% (w/v) PEI/ methanol solution, agitated at 180 rpm at 298 K for 2 h. Later, the mixture was immediately transferred to 200 ml 1% (w/v) glutaraldehyde/methanol solution as cross-linker, sonicated for 2h and further left shaking using a roller (orbital shaker) overnight at room temperature. The solvent was evaporated at room temperature, and the composite formed was called Fe_3O_4–PEI–ACTF, washed with deionized water three times. It was grinding and sieving to constant size.

2.3. Characterization:

Microstructure and surface morphology of the prepared ACTF, Fe_3O_4 NPs, and Fe_3O_4–PEI–ACTF NC was analyzed by using High Resolution Transmission Electron Microscope (HR-TEM model JEOL JEM 2200 FS TEM with a field- emission gun operating at 200 kV), A drop of an aqueous dispersion was placed on a Form var-coated copper TEM grid (300 mesh size) and allowed to air-dry. Furthermore, the structural study of the prepared ACTF, Fe_3O_4 NPs, and Fe_3O_4–PEI–ACTF NC was examined by the wide-angle X-ray diffraction (XRD), using a diffractometer, P analytical X PERT PRO MPD by Cu Kα radiation with (λ= 1.5418 A°) was used at a rating of 40 kV, 40 mA. Functional groups of the synthesized samples ACTF, Fe_3O_4 NPs, and Fe_3O_4–PEI–ACTF NC were identified using a Fourier transform infrared spectrometer (FT-IR) model spectrum one (Perkin Elmer, USA). The samples were prepared as KBr discs and scanned over the range of 400–4000 cm^{-1}. The thermal stability of as prepared ACTF, Fe_3O_4 NPs, and Fe_3O_4–PEI–ACTF NC has been investigated by thermo-gravimetric analysis (TGA, Q600 SDT) from room temperature to 1000°C with a heating rate of 10°C/min under steady nitrogen flow.

2.4. Batch adsorption experiments:

The adsorption capacity of Fe_3O_4–PEI–ACTF NC for Hg(II) metal ions was studied and performed by batch adsorption techniques. The effect of solution pH, initial metal concentration, the adsorbent dose, time and temperature on the adsorption of Hg(II) onto Fe_3O_4–PEI–ACTF NC were investigated. To determine the adsorption isotherm, working Hg(II) solutions ranging from 500 μgL^{-1} to 2000 μgL^{-1} were shaken with a fixed dose of Fe_3O_4–PEI–ACTF NC adsorbent for a specified contact time in a thermo-stated shaking assembly in 50-mL stopper tubes at desired pH at room temperature. At equilibrium, the adsorbent was separated by using external permanent magnet and the supernatant was analyzed for concentration measurements. The adsorption thermodynamics of Hg(II) was carried out at temperatures ranging from 298 K to 343 K. The concentration of Hg(II) was determined according to ASTM D 3223 – 02 standard test method (ASTM). Total mercury in water was analyzed using cold vapor atomic absorption spectrometer (Hitachi model ZEEnit 700P, Germany), attached to hydride system. The system was used for quantitative determination of mercury in liquid samples due to its high sensitivity and selectivity as well as its extremely low detection limits (1 µg/L). Briefly, Hg(II) was reduced to the elemental state using Na B H_4 in presence of argon as a carrier gas, moved through a gas liquid separator. The mercury vapor was enriched on a gold collector, then heated to release elemental mercury which was re-carried out to a quartz cell inside the atomic measurement unit and the concentration of elemental mercury was measured as a function of absorbance. All experiments were carried out in triplicate and average values were calculated.

The adsorption capacity (q_e, $\mu g g^{-1}$), and the removal efficiency percentages were calculated according to the following equations:

$$q_e = (C_0 - C_e)V / m \quad (1)$$

$$\text{Removal efficiency (\%)} = [(C_0 - C_e) / (C_0)] \times 100 \quad (2)$$

C_0 and C_e ($\mu g\ L^{-1}$) are the initial and equilibrium concentrations of Hg(II) metal ions, respectively, V is the volume of solution (L) and m is the mass of the adsorbent (g).

3. RESULTS AND DISCUSSION

3.1. *Characterization:*

The surface morphologies of ACTF, Fe_3O_4 NPs, and Fe_3O_4–PEI–ACTF NC prepared was characterized by HR-TEM images and represented in Fig.1 on different grid areas and different magnifications. The HR-TEM images show that ACTF displayed a platelet-like morphology in the form of thin films with a two-dimensional sheet (Fig.1 a, b), reveals that it consists of multiple accumulated sheets. TEM images of the prepared Fe_3O_4 NPS (Fig.1c, d), reveal that the synthesized nanoparticles are nearly spherical shaped structures, well dispersed in methanol with particle sizes ranged from 10 to 18 nm. The corresponding TEM images of Fe_3O_4–PEI–ACTF NC (Fig.1e, f, g) shows that it has lamellar structure; small groups as well as individual magnetite nanoparticles were found to be dispersed among the ACTF platelets and on their surfaces. Polyethylenimine (PEI) on magnetite surface penetrated into the ACTF platelets producing intercalation, and their penetrating through its

sheets. Since sorption sites are predominantly on the surface, Fe_3O_4–PEI–ACTF NC was expected to offer more active sorption sites on its surface. The Selected Area Electron Diffraction (SAED) Fig.1 h, shows the diffraction rings of polycrystalline nature of Fe_3O_4–PEI–ACTF NC prepared, confirmed the crystallinity and preferential orientation.

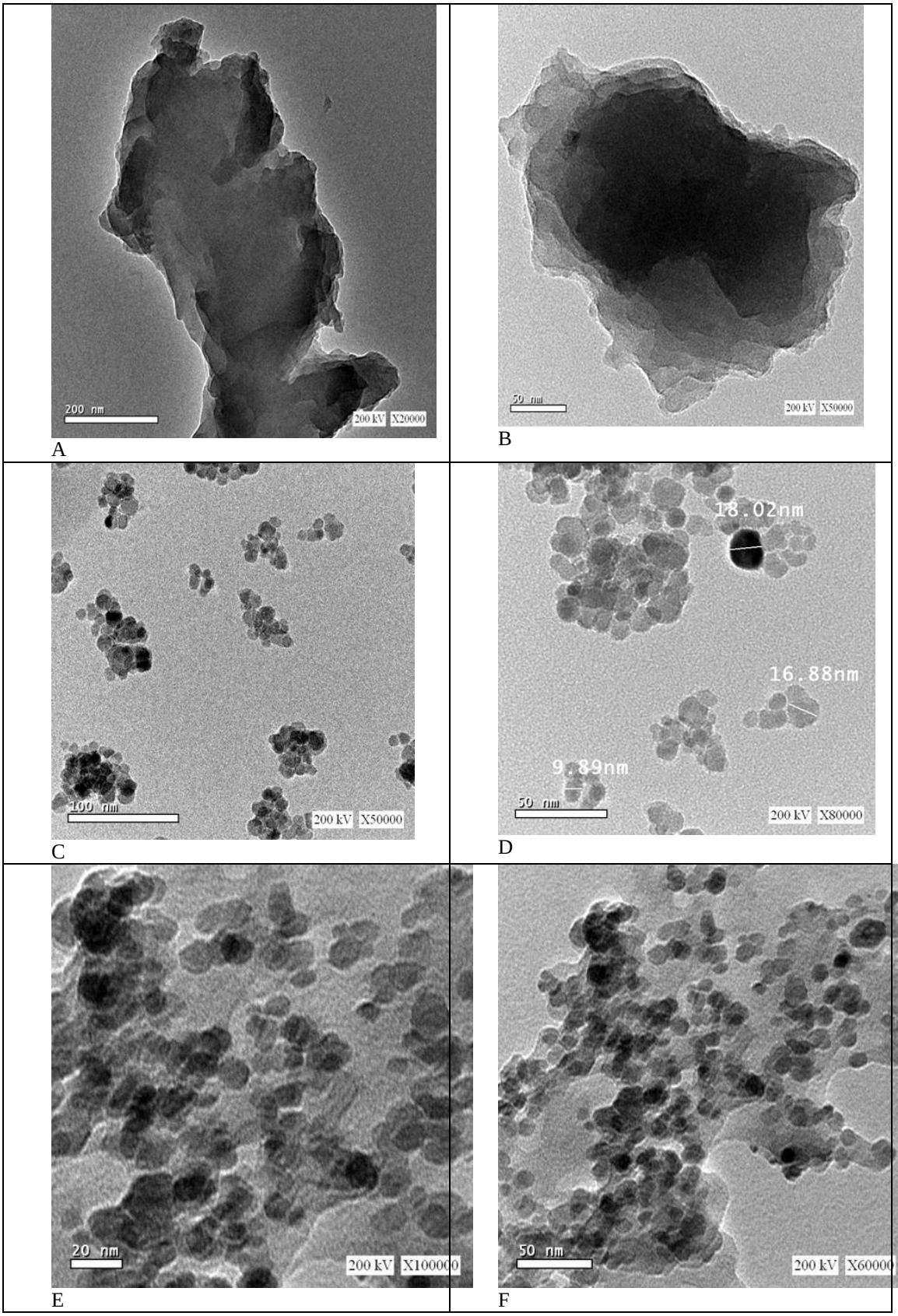

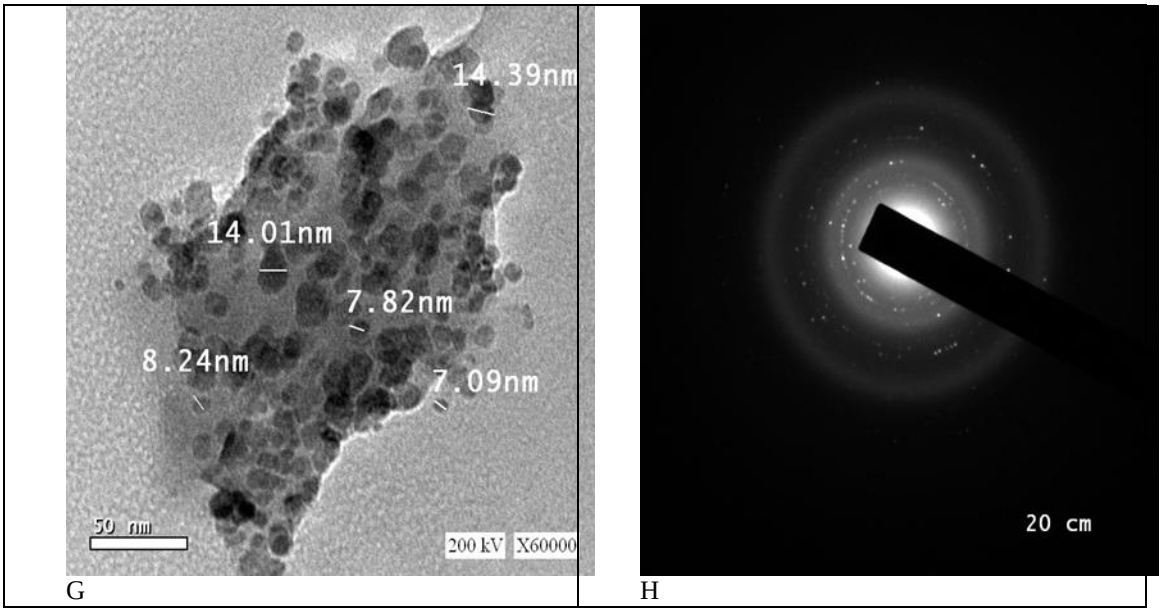

Fig. 1: HR-TEM images of ACTF (a, b), Fe_3O_4 NPs (c, d), Fe_3O_4 -PEI-ACTF N C (e, f, g) on different grid areas and different magnifications, and SAED (h) of composite.

The XRD patterns of the synthesized ACTF, Fe_3O_4NPs, and Fe_3O_4–PEI–ACTF NC were shown in Fig.2. The pattern of ACTF shows that the fabricated activated carbon was amorphous with a broad peak at 2Θ = 21.47◦. While the pattern of Fe_3O_4 NPs shows the characteristic diffraction peaks of Fe_3O_4 at angles (2Θ) = 30.21º, 35.65º, 43.35º, 53.67º, 57.59º, and 63.13º represent the corresponding indices (2 2 0) (3 1 1) (4 0 0)(4 2 2) (5 1 1) and (4 4 0), respectively (Nata et al. 2010, Zhang et al. 2011), which match with the pattern of the standard Fe_3O_4 according to ICDD PDF card (03-0863). The pattern of the Fe_3O_4–PEI–ACTF NC, shows the characterized peaks of ACTF and PEI which can be observed in the area of 2Θ = 19º - 21.5º. Moreover, all the characterized diffraction peaks of Fe_3O_4 NPs were sharply detected due to its high crystalline nature. The results indicate that Fe_3O_4–PEI–ACTF NC was successfully prepared, and confirmed its structure (Xiaoyao *et al.* 2014).

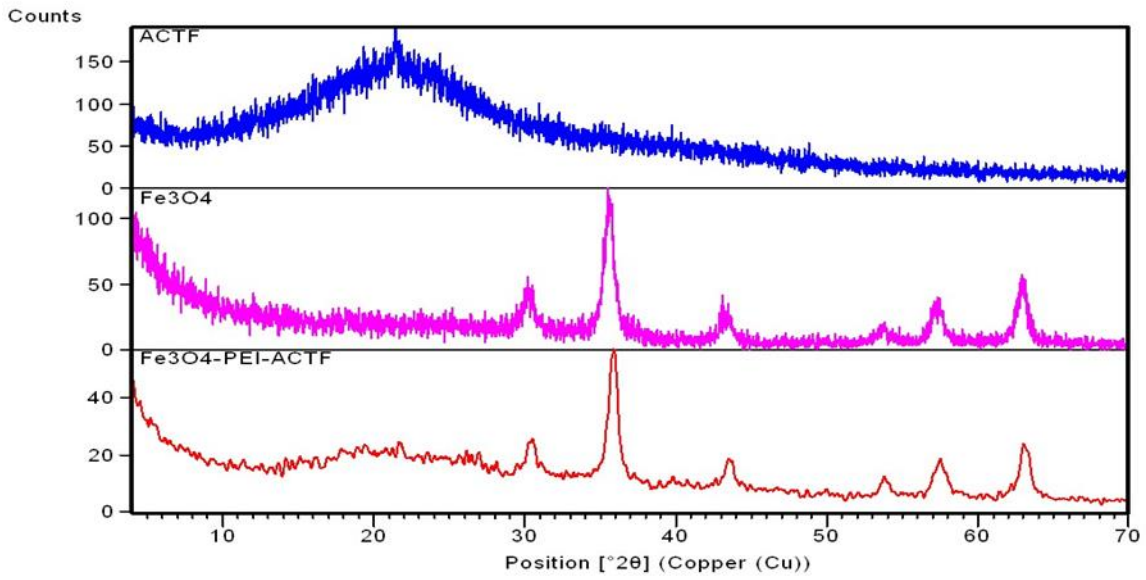

Fig. 2: XRD pattern of ACTF, Fe_3O_4 NPs, and Fe_3O_4-PEI-ACTF NC prepared

The FT-IR spectra of PEI, ACTF, Fe_3O_4 NPs, and Fe_3O_4–PEI–ACTF NC are shown in Fig 3.The spectra revealed the presence of N-H, O-H, C=O, C-C, and C-O bands at 3440 cm^{-1}, 3416 cm^{-1}, 1703 cm^{-1}, 1614 cm^{-1} and 1174 cm^{-1}, respectively. The bands around 2919 and 2850 cm^{-1} are attributed to stretching vibration of the

aliphatic C–H bands. In the spectrum of Fe_3O_4NPs, the strong absorption band at 583 cm^{-1} corresponded to Fe-O bond vibration of Fe_3O_4 (Ai *et al*. 2011; Limei *et al*. 2015). The spectrum of Fe_3O_4–PEI–ACTF NC shows that Fe-O bond vibration of Fe_3O_4 shifted to 620 cm^{-1}, the broad and strong band ranging from 3000 to 3800 cm^{-1} which may be due to the overlapping of OH and NH stretching, while the presence of two absorption bands at 2926 cm^{-1}, and 2850 cm^{-1} corresponds to the CH_3 asymmetric as well as symmetric stretching frequencies of the methyl groups in PEI chains (Xitong *et al*. 2014). In addition, the new characteristic peak appeared at 1636 cm^{-1} corresponding to the bending vibration of (–C(=O) –N(–H)–) (Xitong *et al*. 2014), which implied that the PEI was successfully grafted on the surface of the ACTF and Fe_3O_4 NPs. Fe–O bond vibrating of shifted to about 620 for Fe_3O_4–PEI–ACTF NC. As can be seen in spectrum of Fe_3O_4–PEI–ACTF NC contains all the special peaks of its constituents; ACTF, PEI, and Fe_3O_4. Hence, the FTIR spectrum confirmed that Fe_3O_4–PEI–ACTF NC was successfully prepared and it contained plentiful oxygen and nitrogen functional groups, which act as available adsorption sites, played an important role in the heavy metal ions removing process.

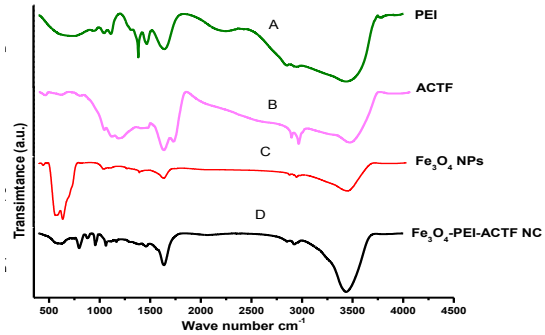

Fig. 3: FTIR spectra of PEI (A), and ACTF (B), Fe_3O_4 NPs (C), and Fe_3O_4-PEI-ACTF NC (D) prepared

Thermal stability is an important factor that affects the application of an adsorbent. The thermal stability of ACTF, PEI, Fe_3O_4NPs, and Fe_3O_4- PEI- ACTF NC was investigated by thermal gravimetric analysis (TGA) in dry nitrogen and in the temperature range from 15 to 1000 ºC. Fig. 4 shows TGA curves of ACTF, PEI, Fe_3O_4NPs, and Fe_3O_4–PEI- ACTF NC, it was clear that Fe_3O_4NPs prepared showed high thermal stability and a little weight loss of 5% was observed within the experimental temperature between 15 ºC to 1000 ºC. For the Fe_3O_4–PEI-ACTF NC the weight losses occurred at three different temperature ranges, the first stage of weight loss ranging from 15 to 125 ºC of about (10%) corresponded to the removal of surface hydroxyl groups and/or adsorbed and bounded water on its surface (Kumar *et al*. 2010; Inbaraj *et al*. 2011; Burks *et al*. 2014), indicating the low content of adsorbed water. The second stage of weight loss of about 38%, beginning at around 125 ºC and completing at about 500 ºC, might be attributed to the thermal degradation of organic components materials including decomposition of functional groups of ACTF and PEI and carbonization of main chains. Since the decomposition of pure PEI occurs at the same temperature range and with the same behavior from 200 ºC to 390 ºC (Inigo *et al*. 2012), the contents of PEI polymer was calculated to be ≈ 24%. At the third stage, from 500 to 700 ºC, there was a small weight loss of about 9% till equilibrium occurs. The Fe_3O_4 NPs content was estimated to be ≈ 28%, indicated that Fe_3O_4–PEI-ACTF NC had magnetic content.

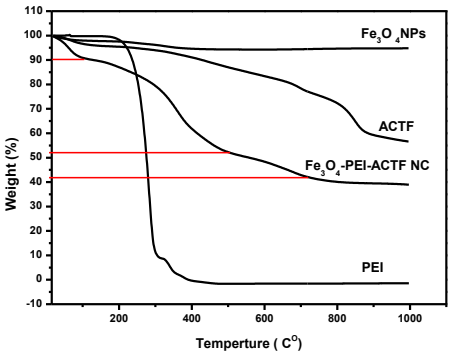

Fig. 4: GTA curves for Fe3O4 NPs, ACTF, and Fe3O4-PEI-ACTF NC materials prepared, and PEI

Australian Journal of Basic and Applied Sciences, 10(18) December 2016, Pages: 323-335

3.2. Effect of pH on adsorption:

The pH of solution is an important parameter for assessing the adsorption efficiency of an adsorbent. Dependence of metal sorption on pH is related to both the metal chemistry in the solution and functional groups of sorbent surface which affects the availability of binding sites (Ho, Y.-S. 2005; Heidari *et al*. 2009). Batch adsorption experiments were performed in a wide range of pH (3–10). The pH was adjusted to the desired pH value by adding negligible amounts of 0.01 M HNO_3 or NaOH. As shown in Fig. 5, the adsorption efficiency % increases with increasing solution pH. In acidic condition, large number of H^+ protonated the amino groups on the surface of Fe_3O_4–PEI–ACTF NC adsorbent and so, repulsion occurs between H^+ protons and Hg^{2+} on the adsorption sites, although competition adsorption of H^+ exists, the affinity of Fe_3O_4–PEI–ACTF NC adsorbent towards Hg^{2+} was higher and still exhibited adsorption efficiency % (over 80 %) at pH about 3. So Fe_3O_4–PEI–ACTF NC adsorbent was suitable for removal mercury not only from neutral solution, but also in low pH solutions. As pH increased, the protonation of $–NH_2$ group decreased and so more $–NH_2$ groups can coordinate with Hg^{2+}, With the further increase of pH, OH^- concentration increased on the adsorbent surface, resulting in a high surface charge density, consequently, an increase in the adsorption efficiency % of Hg(II). At a pH > 9, the colloidal precipitate of $Hg(OH)_2$ was formed, which also decreased the adsorption efficiency %. Therefore, no adsorption experiment was performed at pH > 10. The optimized pH of 5 was selected for Hg(II) in subsequent tests.

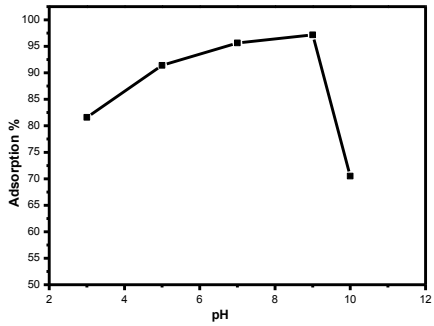

Fig. 5: Effect of pH on the adsorption behavior of Hg(II) on Fe3O4–PEI–ACTF NC adsorbent, m= 0.04 g, V= 0.05 L, Co = 500 µg L-1 and T = 298.15 K

3.3. Effect of adsorbent dose:

The effect of Fe_3O_4–PEI–ACTF NC adsorbent dose on the adsorption capacity of Hg(II) (q_e (µg g^{-1}), as well as the removal efficiency %, were investigated at different dose (0.4 – 1.2 gL^{-1}) and represented in Fig. 6. The dosage of adsorbent determines the contact areas between the adsorbent surface and adsorbate As shown (Fig. 6), the removal efficiency % of Hg(II) increased from 78.2 % to 95.4 % with the increase of adsorbent dosage from 0.4 g to 1.2 g. The increase of removal efficiency % may be attributed to increases in the adsorbent surface area and consequently the number of adsorption sites available for the adsorption and the number of functional groups at Fe_3O_4–PEI–ACTF NC adsorbent surface increases. The adsorption capacity of Hg(II) on Fe_3O_4–PEI–ACTF composite adsorbent decreases gradually with the increase of solid content (Donglin *et al*. 2011). This may be attributed to the increase ratio of net adsorption quantity of Hg(II) on Fe_3O_4–PEI–ACTF NC surface is lower than that of the solid content, correspondingly, decreasing the adsorption capacity of Hg(II) on Fe_3O_4–PEI–ACTF NC.

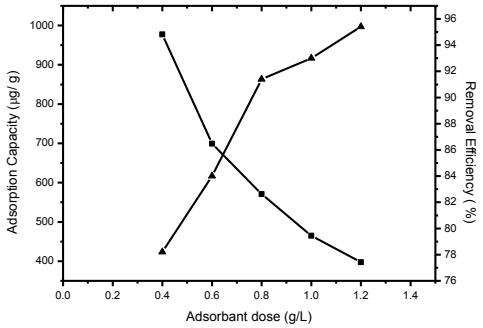

Fig. 6: Adsorbent capacity and removal efficiency % of Hg(II) on Fe3O4–PEI–ACTF NC adsorbent as a function of adsorbent dose, V= 0.05 L, Co = 500 µgL-1 and T =298.15 K

Australian Journal of Basic and Applied Sciences, 10(18) December 2016, Pages: 323-335

3.4. Effect of initial metal ion concentration and adsorption isotherms:

The effect of initial mercury ion concentration on the Hg(II) removal efficiency %, adsorption experiments were performed with initial Hg(II) concentrations that ranged from 500 μgL^{-1} to 2000 μgL^{-1}. An amount of 0.04 g of Fe_3O_4–PEI–ACTF NC adsorbent was added to 0.05 L, under conditions of pH = 5, a stirring speed of 180 rpm, 2 h of contact time and at room temperature was used for each adsorption experiment. The removal efficiency % was presented in Fig. 7, which shows that the removal efficiency % decreased from 91.4% to 28.3%, with increased initial Hg (II) concentration from 500 to 2000 µg L^{-1}. These results indicate that the adsorption is dependent on the Hg(II) concentration as it provides the main driving force to overcome mass transfer limitations between the solid and the aqueous phase. At lower concentration, a greater number of active sites are available for adsorption, and consequently the adsorption is independent on the initial metal ion concentration. At a high metal ion concentration, the number of available adsorption sites on adsorbent surface deceased, get saturated, and further mass transfer from liquid phase comes down for a fixed number of active sites on adsorbent versus to increase metal ions concentration and the extent of adsorption decreased (Ali *et al*. 2015).

The relationship between the metal ions adsorbed on the surface of adsorbent and those remaining in the aqueous phase was studied and the adsorption isotherm data were analyzing by Langmuir and Freundlich isotherm models

The Langmuir isotherm model assumes a monolayer adsorption of metals and all adsorption sites are identical and energetically equivalent. Its linear form is expressed by the following equation:

$$\frac{C_e}{q_e} = \frac{1}{b\,q_{max}} + \frac{C_e}{q_{max}} \quad (3)$$

Where, C_e is the equilibrium metal ions concentration in the solution (µg L^{-1}); q_e is the equilibrium metal ions concentration per unit mass of adsorbent (µg g^{-1}); q_{max}, the maximum adsorption capacity, is the amount of metal ions at complete monolayer coverage (µg g^{-1}); and b ($L\mu g^{-1}$) is the Langmuir constant related to energy of adsorption. Langmuir parameters, q_{max} and b are determined from the slope and intercept of the linear relationship plotting between C_e/q_e versus C_e (Fig. 8) and listed in Table. 1

The favorability of Hg(II) metal ions adsorption onto Fe_3O_4–PEI–ACTF composite was evaluated by dimensionless constant R_L called the separation factor or equilibrium parameter, derived from Langmuir model. Values of R_L indicate the shapes of isotherms to be either unfavorable (R_L> 1), linear (R_L = 1), favorable (0 < R_L<1) or irreversible (R_L = 0) (Weber and Chakkravorti 1974).

$$R_L = \frac{1}{1+bC_o} \quad (4)$$

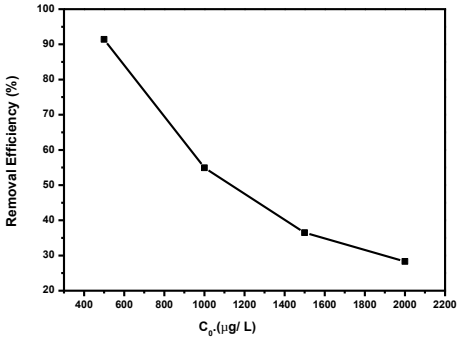

Fig. 7: Removal efficiency % of Hg(II) on Fe3O4–PEI–ACTF NC adsorbent as a function of initial metal concentration, V= 0.05 L, m = 0.4 g and T =298.15 K

The Freundlich isotherm model is considered for describing both multilayer sorption and sorption on heterogeneous surfaces suggesting that binding sites are not equivalent and/or independent. The logarithmic form of Freundlich isotherm is described by the following equation:

$$\log q_e = \frac{1}{n} \log C_e + \log K_f \quad (5)$$

Where, K_f represented the adsorption capacity when metal ion equilibrium concentration equals to 1, and n the empirical constant depicting the intensity of adsorption which varies with the heterogeneity of the adsorbent. The greater is the value of n the better its adsorption capacity. Freundlich constants K_f and n are calculated from the plot of log q_e versus log C_e (Fig. 8) and listed in Table 1.

The best-fit of the experimental data to both models was determined on the basis of regression correlation coefficients $R^{2,}$ listed in Table 1. The correlation coefficients analysis shows that adsorption of Hg (II) on Fe_3O_4–PEI–ACTF NC adsorbent well fitted with the Langmuir model as compared to the Freundlich model, indicating that the binding energy on the whole surface of adsorbent is uniform and the whole surface has

Table 1: Langmuir, and Freundilch isotherm parameters and correlation coefficients for adsorption of Hg(II) onto Fe_3O_4–PEI–ACTF NC adsorbent

Langmuir isotherm				Freundilch isotherm		
q_{max}(µg/g)	b	R_L	R^2	K_F	n	R^2
714	0.0596	0.0083-0.0325	0.9995	458.1	16.39	0.951

identical adsorption activity. The adsorbed Hg(II) metal ions forming an almost complete monolayer coverage of Fe_3O_4–PEI–ACTF NC adsorbent, and the maximum adsorption capacity (q_{max}) was 714 µg g^{-1}.

As listed in Table 1, all R_L values are in the range of 0.0083 to 0.0325, over all initial concentration (500 – 2000 µg/L), implies that the adsorption of Hg(II) metal ions onto Fe_3O_4–PEI–ACTF NC adsorbent was favorable under the operating conditions being studied.

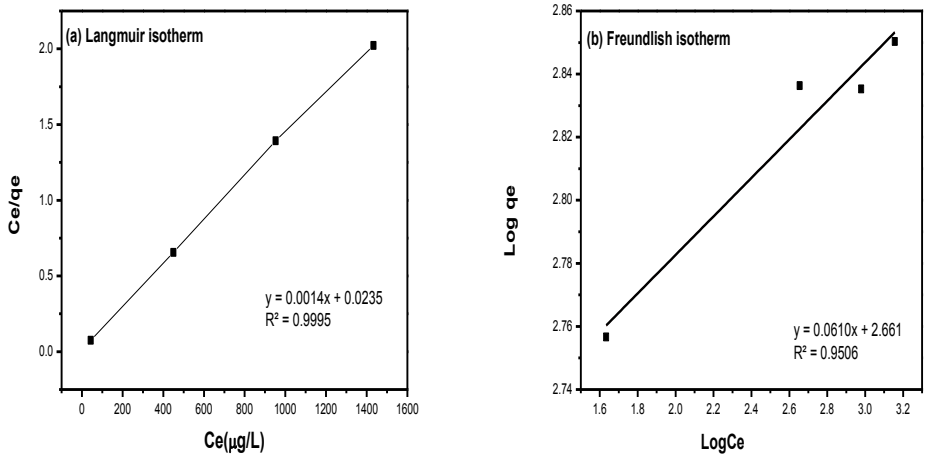

Fig. 8: Langmuir adsorption isotherm model (a), and Freundlich adsorption isotherm model (b) fitting Hg(II) adsorption onto Fe_3O_4–PEI–ACTF NC adsorbent, m = 0.04g, V= 0.05 L, C_o = 500 – 2000 µg L^{-1} and T= 298.15 K.

3.5. Effect of contact time and adsorption kinetics:

The effect of contact time on the adsorption of Hg(II) was investigated at 500 µg L^{-1} initial concentration at optimum adsorbent dose (0.04 g/0.05L) at pH 5.0. As shown in Fig. 9, the adsorption rate was initially very high and 83 % of maximum uptake of Hg(II) removed takes place at 30 min, then slowed down as the equilibrium approached and maximum uptake of 575 µg Hg(II)/g was obtained after 90 min. In order to investigate the kinetics of the adsorption process, the pseudo-first-order and pseudo-second-order kinetic models were applied to describe the rate of Hg(II) uptake on the Fe_3O_4–PEI–ACTF NC adsorbent (Fig. 10).

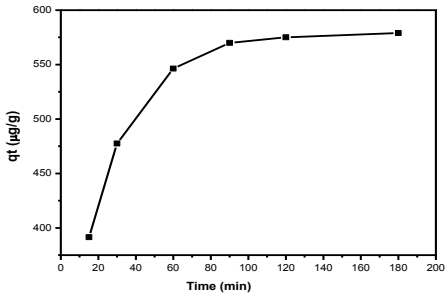

Fig. 9: Effect of time on adsorbtion of Hg(II) onto Fe3O4–PEI–ACTF NC adsorbent, m = 0.04g, V= 0.05 L, Co = 500 µg L-1 and T= 298.15 K .

1. The pseudo-first-order Lagergren'smodel (Ho, Y.-S., 2004):

$$\log(q_e - q_t) = \log q_e - \frac{K_1}{2.303}t \quad (6)$$

2. The pseudo-second order model (Ho, Y.-S., 2006):

$$\frac{t}{q_t} = \frac{1}{K_2 q_e^2} + \frac{1}{q_e}t \quad (7)$$

q_e and q_t are the capacity of metal ions adsorbed (mg g^{-1}) at equilibrium and time t (h), respectively, k_1 is the pseudo-first- order rate constant (h^{-1}), and K_2 (g $mg^{-1}h^{-1}$) is the pseudo-second order rate constant.

The kinetic rate constants for the adsorption of Hg (II) on Fe_3O_4–PEI–ACTF NC composite were determined by the linear regression analysis and the results are summarized in Table 2. According to the R^2 values, the experimental data fit the pseudo-second-order kinetic model better than the pseudo-first-order kinetic model. The R^2 values obtained from the pseudo-second-order model are > 0.999 and the calculated equilibrium adsorption capacities (qe, 606 µg/g) were consistent with the experimental (qe, 575 µg/g). The second-order kinetics suggests that the adsorption is a chemisorption process, indicating that electrostatic attraction are the main driving force for the adsorption and coordination occurred between the metal ions and PEI-functionalizing magnetic amorphous carbon (Lu *et al*. 2015). This result can be attributed to the active oxygen and nitrogen functional groups, which act as available adsorption sites and played an important role in the heavy metal ions removing process.

Table 2: The kinetic parameters and correlation coefficients for adsorption of Hg(II) onto Fe_3O_4–PEI–ACTF NC adsorbent

q_e, exp.(µg/g)	Pseudo-first-order kinetic model			Pseudo-second-order kinetic model		
575	$q_{e,\ calc.}$(µg/g)	K1(min^{-1})	R^2	$q_{e,\ calc.}$(µg/g)	K2(g/ µg min)	R^2
	442.588	0.0499	0.993	606.06	0.00023	0.9996

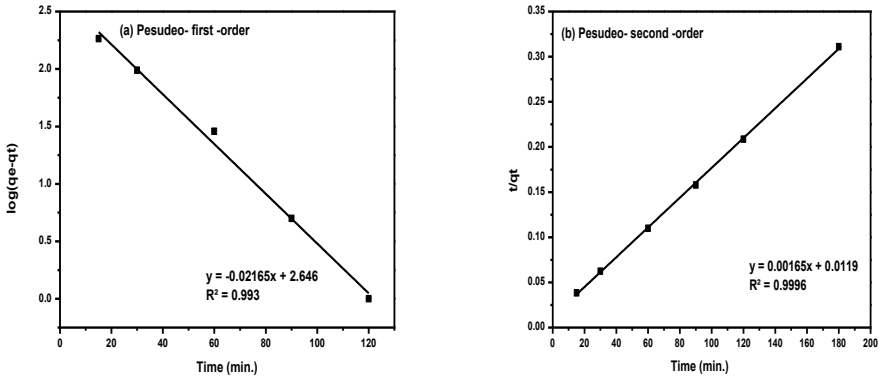

Fig. 10: Pseudo-first order (a) and Pseudo-second order (b) kinetic plots of Hg(II) adsorption onto Fe_3O_4–PEI–ACTF NC adsorbent, m = 0.04g, V= 0.05 L, C_o = 500 µg L^{-1} and T= 298.15 K

3.5. Effect of temperature and thermodynamic parameters:

Temperature is an important factor that affects the adsorption process. In this work, the effect of the temperature on the adsorption performance of mercury onto Fe_3O_4–PEI–ACTF NC adsorbent was evaluated over the temperature range of 288–308 K at initial Hg(II) concentration of 500 µg /L. The thermodynamic parameters, namely ΔG^o(kJ mol^{-1}) is the Gibbs free energy change, ΔS^o (J mol^{-1} K^{-1}) is the entropy change, $and\ \Delta H^o$ (kJ mol^{-1}) is the enthalpy change were obtained from van't Hoff equations (Eq. 8 -11) and the results are listed in Table.3

Table 3: Thermodynamic data for adsorption of Hg(II) onto Fe_3O_4–PEI–ACTF NC adsorbent

ΔG^o(KJ mol^{-1}) at different temperature T (K)			$\Delta H^o(KJ\ mol^{-1})$	$\Delta S^o(KJ$ mol^{-1} $K^{-1})$
288	298	308		
- 4.2784	-6.4060	- 8.1591	51.763	0.1948

$$K_d = q_e / C_e \quad (8)$$

$$\Delta G^o = -RTlnK_d \quad (9)$$

$$\Delta G^o = \Delta H^o - T\Delta S^o \quad (10)$$

$$lnKd = -\frac{\Delta G^o}{RT} = \frac{\Delta S^o}{R} - \frac{\Delta H^o}{RT} \quad (11)$$

R (8.314 J mol^{-1} K^{-1}) is the gas constant, T (K) is temperature Kelvin, K_d is the distribution coefficient, q_e is the amount of metal ion adsorbed at equilibrium (µg/g) and C_e is the equilibrium concentration of metal ions in the solution (µg/L). The values of ΔG^o is calculated from Eq. 9 and the values of ΔS^o and ΔH^o are obtained (Eq. 10) from the intercept and slope of van't Hoff plot (Fig. 11) of $lnKd$ versus 1/T, respectively. Positive values of ΔH^o confirm the endothermic nature of adsorption process of mercury (II) onto Fe_3O_4–PEI–ACTF NC adsorbent and the adsorption efficiency increase with temperature. The more negative values of ΔG^o indicates the more spontaneous nature of adsorption of mercury(II). The positive value of ΔS^o suggests that the adsorbed mercury (II) ions remain more randomly over the adsorbent surface. The adsorbed water molecules, which were

displaced by the metal ions, gained more translational entropy than were lost by the metal ions, thus allowing the increase of randomness in the system (Fan *et al*. 2012). Improving the adsorption capacity with temperature suggests that active centers on the surface available for adsorption increase with the temperature. This could also be attributed to the pore size variation and enhancing rate of intraparticle diffusion of solute since diffusion is an endothermic process. Also, Giles *et al*. 1974, believed that high temperatures increase the mobility of the mercuric ion and widen the pore on the adsorbent surface leading to enhanced intra-particle diffusion rate, which reveals a physical nature of the adsorption process (Pejman *et al*. 2015).

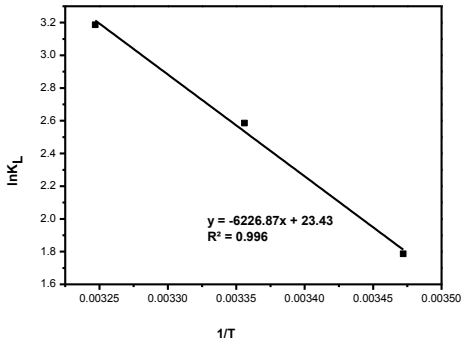

Fig. 11: Effect of temperature on the adsorption of Hg(II) adsorption onto Fe3O4–PEI–ACTF NC adsorbent, m = 0.04g, V= 0.05 L, Co = 500 µg L-1

Conclusions:

In this study, polyethylenimine (PEI) functionalized magnetic amorphous carbon nano composite (Fe_3O_4-PEI-AC NC), has been synthesized in a simple method, and characterized by High Resolution Transmission Electron Microscope (HR-TEM), Fourier-transform infrared spectrometer (FTIR), X-ray diffraction (XRD), and TGA. Results confirmed that Fe_3O_4–PEI–ACTF NC was successfully prepared, and it contained plentiful oxygen and nitrogen functional groups, which act as available adsorption sites. The efficiency of Fe_3O_4-PEI-ACTF NC to remove Hg (II) from aqueous solution was investigated in a batch system. Adsorption experiments demonstrated that Fe_3O_4-PEI-ACTF NC exhibited excellent adsorption performance for Hg(II), which may be attributed to the coordination property of PEI and the electrostatic interaction between Hg(II) and oxygen and nitrogen functional groups on its surface. Results showed that the adsorption efficiency increased by an increase in the temperature and the adsorbent dosage as well as a decrease in the initial Hg (II) metal concentration. The adsorption kinetic follows the pseudo-second-order model and the adsorption isotherm could be fitted well with Langmuir model which suggests that the adsorption is a chemisorption process and electron transfer, exchange or sharing was generated and chemical bond was formed in the process. The calculated thermodynamic parameters revealed that the adsorption of Hg(II) onto Fe_3O_4-PEI-ACTF NC is endothermic and spontaneous in nature. The results of this study indicated that Fe_3O_4-PEI-ACTF NC could be satisfactorily used in practical application for removing heavy metals from aqueous environments due to high adsorption capacity and easily and quick separation.

REFERENCES

Ai, L., C. Zhang, Z. Chen, 2011, J. Hazard. Mater. 192: 1515-1524.

Ali Azari, Babak Kakavandi, Roshanak Rezaei Kalantary, Ehsan Ahmadi, Mitra Gholami, Zahra Torkshavand, Minoo Azizi, 2015, J Porous Mater 22: 1083-1096.

AMERICAN SOCIETY FOR TESTING AND MATERIALS (ASTM) Standard Test Method for Total Mercury in Water, D 3223-02.

Bagheri, H., A. Afkhami, M. Saber-Tehrani, H. Khoshsafar, 2012. Talanta, 97: 87.

Burks, T., M. Avila, F. Akhtar, M. Gothelid, P.C. Lans•ker, M.S. Toprak, M. Muhammed, A. Uheida, 2014. Journal of Colloid and Interface Science., 425: 36-43.

Ch. Wang, Sh. Tao, W. Wei, Ch. Meng, F. Liua, M. Han 2010, J. Mater. Chem., 20: 4635.

Cheng, G., M. He, H. Peng, B. Hu, 2012. Talanta, 88: 507.

Deng, S.B., Y.P. Ting, 2005. Water Res., 39: 2167-2177.

Donglin, Z., S. Guodong, H. Jun, C. Changlun, W. Xiangke, 2011. Chemical Engineering Journal, 171: 167-174.

El-Sayed, M., M. Ramzi, R. Hosny, M. Fathy and Th. Abdel Moghny, 2016, Water Science & Technology, 73(10): 2361-2369.

Fan, H.-T., J.-B. Wu, X.-L. Fan, D.-S. Zhang, Z.-J. Su, F. Yan, T. Sun, 2012. Chem. Eng. J., 355: 198-199.

Ghoul, M., M. Bacquet, M. Morcellet, 2003. Water Res, 37: 729-734.

Giles, C.H., D.S mith, A.H uitson, 1974. J. Colloid Interface Sci., 47: 755.

Hajipour, A.R., S. Habibi, A.E. Ruoho 2010, J. Appl. Polym. Sci., 118: 818-826.

Harris, H.H., I.J. Pickering, G.N. George, 2003. Science, 301: 1203.

Heidari, A., H. Younesi, Z. Mehraban, 2009. Chem. Eng. J. 153: 70-79.

Ho, Y.-S., 2004. Scientometrics, 59: 171-177.

Ho, Y.-S., 2005. Bioresour. Technol., 96: 1292-1296.

Ho, Y.-S., 2006. J. Hazard.Mater., 136: 681-689.

Inbaraj, B.S., T.H. Kao, T.Y. Tsai, C.P. Chiu, R. Kumar, B.H. Chen, 2011. Nanotechnology, 22: 075101/1-9.

Inigo Larraza, Mar Lopez-Gonzalez, Teresa Corrales, Gema Marcelo, 2012. Journal of Colloid and Interface Science., 385: 24-33.

Jianga, H., Zh. Yan, Y. Zhao, X. Hu, H. Lian, 2012. Talanta, 94: 251.

Kumar, R., B.S. Inbaraj, B.H. Chen, 2010. Mater. Res. Bull., 45: 1603-1607.

Limei Cui, Yaoguang Wang, Liang Gao, Lihua Hu, Liangguo Yan, Qin Wei, Bin Du, 2015. Chemical Engineering Journal, 281: 1-10.

Lu, H., L. Dan-Dan, W. Bing-Bing, X. Hong-Bo, 2015. Res Chem Intermed, 41: 3913-3928.

Mohapatra, S., D. Pal, S.K. Ghosh, P.P. Pramanik 2007, J. Nanosci. Nanotechnol., 7: 3193.

Nasirimoghaddam, S., S. Zeinali, S. Sabbaghi, 2015. Journal of Industrial and Engineering Chemistry, 27: 79.

Nata, I.F., G.W. Salim, C.-K. Lee 2010, J. Hazard. Mater., 183: 853-858.

Pang, Y., G. Zeng, L. Tang, Y. Zhang, Y. Liu, X. Lei, Z. Li, J. Zhang, G. Xie, 2011b. Desalination 281: 278-284.

Pang, Y., G.Z eng, L. Tang, Y.Z hang, Y.L iu, X. Lei, Z. Li, J. Zhang, Z. Liu, Y. Xiong, 2011a. Chem. Eng. J. 175: 222-227.

Panneerselvam, P., N. Morad, K.A. Tan 2011, J. Hazard. Mater. 186: 160.

Parham, H., B. Zargar, R. Shiralipour 2012, J. Hazard. Mater, 205-206: 94.

Pejman Hadi, Ming-Ho To, Chi-Wai Hui, Carol Sze Ki Lin, Gordon McKay, 2015. water research, 73: 37.

Wang, W.Q., C.C. Li, J.L. Yao, B. Zhang, Y.T. Zhang, J.D. Liu 2013, J. Mol. Liq. 184: 10-16.

Weber, T.W., R.K. Chakkravorti, 1974. AlChE J. 20: 228-238.

Xiaofang Shen, Qin Wang, WenLing Chen, Yuehong Pang, 2014. Applied Surface Science, 317: 1028-1034

Xiaoyao Guo, Bin Du, Qin Wei, Jian Yang, Lihua Hu, Liangguo Yan, Weiying Xu, 2014. Journal of Hazardous Materials, 278: 211-220.

Xitong, S., Y. Liangrong, L. Qian, L. Zhini, D. Tingting, L. Huizhou, 2015. Chemical Engineering Journal 262: 101-108.

Xitong, S., Y. Liangrong, X. Huifang, Z. Junmei, L. Xiaopei, H. Yinbin, L. Huizhou, 2014. Colloids and Surfaces A: Physicochem. Eng. Aspects, 457: 160-168.

Ying, M., L. Wu-Jun, Z. Nan, L. Yu-Sheng, J. Hong, S. Guo-Ping, 2014. Bioresource Technology, 169: 403-408.

Yong-Meia, H., Ch. Man, H. Zhong-Bo 2010, J. Hazard. Mater.184: 392.

Zhang, Y., X. Liu, J. Nie, L. Yu, Y. Zhong, C. Huang, 2011. J. Solid State Chem, 184: 387-390.

Zhou, L., Y. Wang, Zh. Liu, Q. Huang 2009, J. Hazard. Mater., 161: 995.